

000
001
002054
055
056003

External Prior Guided Internal Prior Learning for Real Noisy Image Denoising

057
058004
005
006
007
008
009
010
011059
060
061
062
063
064
065

Anonymous CVPR submission

Paper ID 1047

012

Abstract

066

013 Most of existing image denoising methods use some
014 statistical models such as additive white Gaussian noise
015 (AWGN) to model the noise, and learn image priors from ei-
016 ther external data or the noisy image itself to remove noise.
017 However, the noise in real-world noisy images is much more
018 complex than AWGN, and it is hard to be modeled by simple
019 analytical distributions. Therefore, many state-of-the-art
020 denoising methods in literature become much less effective
021 when applied to real noisy images. In this paper, we develop
022 a robust denoiser for real noisy image denoising without
023 explicit assumption on noise models. Specifically, we first
024 learn external priors from a set of clean natural images,
025 and then use the learned external priors to guide the learn-
026 ing of internal latent priors from the given noisy image. The
027 proposed method is simple yet highly effective. Experiments
028 on real noisy images demonstrate that it achieves much bet-
029 ter denoising performance than state-of-the-art denoising
030 methods, including those designed for real noisy images.

067

034

1. Introduction

068

035 Image denoising is a crucial and indispensable step to
036 improve image quality in digital imaging systems. In par-
037 ticular, with the decrease of size of CMOS/CCD sensors,
038 noise is more easily to be corrupted and hence denoising is
039 becoming increasingly important for high resolution imag-
040 ing. In literature of image denoising, the observed noisy im-
041 age is usually modeled as $y = x + n$, where x is the latent
042 clean image and n is the corrupted noise. Numerous image
043 denoising methods [1, 2, 3, 4, 5, 6, 7, 8, 9, 10, 11, 12, 13]
044 have been proposed in the past decades, including sparse
045 representation and dictionary learning based methods [1, 2],
046 nonlocal self-similarity based methods [3, 4, 5, 6, 7], low-
047 rank based methods [8], neural network based methods [9],
048 and discriminative learning based methods [10, 11].

069

049 Most of the existing denoising methods [1, 2, 3, 4, 5, 6, 7,
050 8, 9, 10, 11, 12, 13] mentioned above assume noise n to be
051 additive white Gaussian noise (AWGN). Unfortunately, this
052 assumption is too ideal to be true for real-world noisy im-

053 ages, where the noise is much more complex than AWGN
[14, 15] and varies by different cameras and camera settings
054 (ISO, shutter speed, and aperture, etc.). According to [15],
055 the noise corrupted in the imaging process [is signal depen-
056 dent and comes from five main sources: photon shot, fixed
057 pattern, dark current, readout, and quantization noise. As a
058 result, many advanced denoising methods in literature be-
059 comes much less effective when applied to real-world noisy
060 images. Fig. 1 shows an example, where we apply some rep-
061 resentative and state-of-the-art denoising methods, includ-
062 ing CBM3D [5], WNNM [8], MLP [9], CSF [10], and TRD
063 [11], to a real noisy image (captured by a Nikon D800 cam-
064 era with ISO is 3200) provided in [14]. One can see that
065 these methods either remain the noise or over-smooth the
066 image details on this real noisy image.

067 There have been a few methods [17, 18, 21, 14, 19, 20,
068 22] developed for real noisy image denoising. Almost all of
069 these methods follow a two-stage framework: first estimate
070 the parameters of the assumed noise model (usually Gaus-
071 sian or mixture of Gaussians (MoG)), and then perform de-
072 noising with the estimated noise model. Again, the noise in
073 real noisy images is very complex and hard to be modeled
074 by explicit distributions such as Gaussian and MoG. Fig. 1
075 also shows the denoised results of two state-of-the-art real
076 noisy image denoising methods, Noise Clinic [19, 20] and
077 Neat Image [22]. One can see that these two methods do
078 not perform well on this noisy image either.

079 This work aims to develop a robust solution for real noisy
080 image denoising without explicitly assuming certain noise
081 models. To achieve this goal, we propose to first learn im-
082 age priors from external clean images, and then employ the
083 learned external priors to guide the learning of internal la-
084 tent priors from the given noisy image. The flowchart of
085 the proposed method is illustrated in Fig. 3. We first extract
086 millions of patch groups from a set of high quality natu-
087 ral images, with which a Gaussian Mixture Model (GMM)
088 is learned as the external prior. The learned GMM prior
089 model is used to cluster the patch groups extracted from
090 the given noisy image, and then a hybrid orthogonal dictio-
091 nary (HOD) is learned as the internal prior for image de-
092 noising. Our proposed denoising method is simple and ef-
093

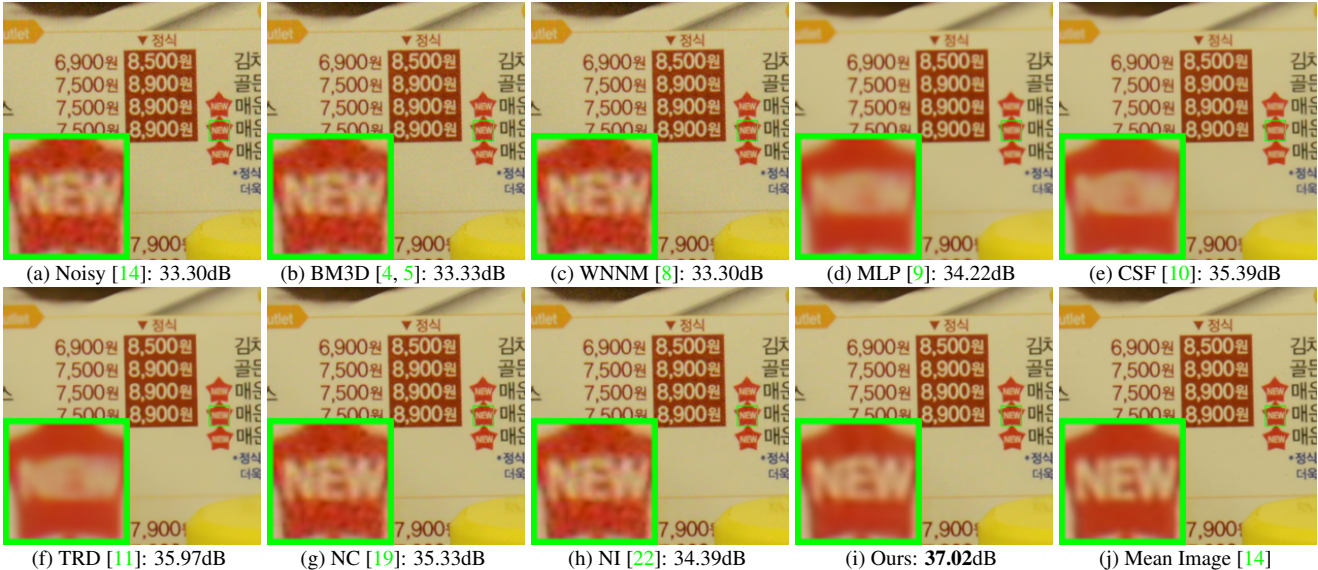


Figure 1. Denoised images of the real noisy image “Nikon D800 ISO 3200 A3” from [14] by different methods. The images are better viewed by zooming in on screen.

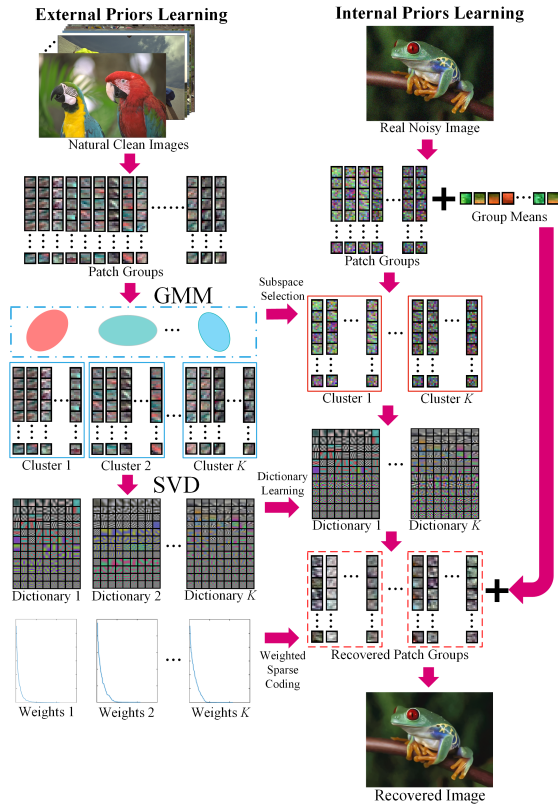


Figure 2. Flowchart of the proposed external prior guided internal prior learning and real noisy image denoising framework.

ficient, yet our extensive experiments on real noisy images clearly demonstrate its better denoising performance than the current state-of-the-arts.

2. Related Work

2.1. Internal vs. External Prior Learning

Image priors are playing key factors in image denoising methods [3, 1, 13, 7, 23]. There are mainly two categories of prior learning methods: 1) External methods pre-learned priors (e.g., dictionaries) from a set of clean images, and the learned priors are used to recover the noisy images [13, 7]. 2) Internal methods directly learned priors from the given noisy image, and the image denoising is simultaneously done with the learning process [1, 24]. On one hand, the methods of [13, 7] demonstrated that the external priors learned from natural clean images are highly effective and efficient for image denoising problem. On the other hand, the work of [6, 23] showed that the internal priors are highly effective for removing the signal independent Gaussian noise. However, the actual noise in real noisy images are much more complex than Gaussian noise. Only using the internal information may be not enough for real image denoising problem. The methods using only the external priors are not adaptive to given real noisy images, while the methods exploiting only internal priors would be degraded by the complex noise. In this paper, we propose to combine both the external and internal priors to solve the real noisy image denoising problem.

2.2. Real Image Denoising

In the last decade, researchers proposed many methods [17, 18, 19, 20, 21, 14] for blind image denoising problem. Liu *et al.* [17] proposed to use “noise level function” to estimate the noise and then use Gaussian conditional random field to obtain the latent clean image. Gong et al. [18] m

216
217
218
219
220
221
222
223
224
225
226
227
228
229
230
231
232
233
234
235
236
237
238
239
240
241
242
243
244
245
246
247
248
249
250
251
252
253
254
255
256
257
258
259
260
261
262
263
264
265
266
267
268
269

odels the noise by mixed ℓ_1 and ℓ_2 norms and remove the noise by sparsity prior in the wavelet transform domain. Recently, Zhu et al. proposed a Bayesian model [21] which approximates and removes the noise via low-rank mixture of Gaussians. The method of “Noise Clinic” [19, 20] and the software of Neat Image [22] are developed specifically for real noisy image denoising. “Noise Clinic” [19, 20] generalizes the NL-Bayes model [25] to deal with blind noise and achieves state-of-the-art performance. However, these methods largely depends on the modeling of noise in real noisy images which is hard to be modeled by explicit distributions. Besides, the parametric estimation of the Gaussian or MoG distribution is often time consuming.

3. External Prior Guided Internal Prior Learning

In this section, we formulate the framework of external patch group (PG) prior guided internal prior learning. We first introduce the external PG prior leaning on natural clean RGB images. Then we propose to employ the learned external PG prior to guide the internal prior (subspace selection and dictionary learning (DL)) learning of given degraded (such as noisy) images. Under the weighted sparse coding framework, the internal prior learning process has alternative closed-form solutions in term of updating sparse coefficients and orthogonal dictionary. Finally, we discuss in details how external prior learned from natural clean images guide the internal prior learning of given degraded (noisy) images.

3.1. Learn External Patch Group Prior

In this section, we formulate the Patch Group prior learned on natural color images. Similar to [7], the patch group (PG) is defined as a group of similar patches to the local patch. The patch group mean is subtracted, and hence different groups of patches can share similar PGs. In this way, the space natural image patches to be modeled is largely reduced.

In this work, each local patch extracted from RGB images is of size $p \times p \times 3$. Then we search the M most similar patches $\{\mathbf{x}_m\}_{m=1}^M$ around each local patch through Euclidean distance, in a local window of size $W \times W$. The $\mathbf{x}_m \in \mathbb{R}^{3p^2 \times 1}$ is a patch vector formed by combining the 3 patch vectors (of size $p^2 \times 1$) in R, G, B channels. The mean vector of this PG is $\boldsymbol{\mu} = \frac{1}{M} \sum_{m=1}^M \mathbf{x}_m$, and the group mean subtracted PG is defined as $\bar{\mathbf{X}} \triangleq \{\bar{\mathbf{x}}_m = \mathbf{x}_m - \boldsymbol{\mu}\}, m = 1, \dots, M$. Assume we have extracted N PGs from a set of external natural images, and the n -th PG is defined as $\bar{\mathbf{Y}}_n \triangleq \{\bar{\mathbf{y}}_{n,m}\}_{m=1}^M, n = 1, \dots, N$. We employ the Gaussian Mixture Model (GMM) to learn the external patch group based NSS prior. The overall objective log-likelihood func-

tion of GMM is

$$\ln \mathcal{L} = \sum_{n=1}^N \ln \left(\sum_{k=1}^K \pi_k \prod_{m=1}^M \mathcal{N}(\bar{\mathbf{x}}_{n,m} | \boldsymbol{\mu}_k, \boldsymbol{\Sigma}_k) \right). \quad (1)$$

The learning process is similar to the learning stage of the PGPD method [7]. Please refer to [7] for more details. After the learning stage, we finally obtain a GMM model with K Gaussian components. The learned parameters include mixture weights $\{\pi_k\}_{k=1}^K$, mean vectors $\{\boldsymbol{\mu}_k\}_{k=1}^K$, and covariance matrices $\{\boldsymbol{\Sigma}_k\}_{k=1}^K$. Similar to [7], the mean vector of each cluster is natural zeros, i.e., $\boldsymbol{\mu}_k = \mathbf{0}$.

Now, we have clustered the PGs extracted from external clean images into K Gaussians or subspaces. To better characterize each subspace, we perform singular value decomposition (SVD) on the covariance matrix:

$$\boldsymbol{\Sigma}_k = \mathbf{U}_k \mathbf{S}_k \mathbf{U}_k^\top. \quad (2)$$

The singular vector matrices $\{\mathbf{U}_k\}_{k=1}^K$ are employed as the external orthogonal dictionary to guide the internal dictionary learning. In Figure 4 (a) and (b), we illustrate an external clean image and one orthogonal dictionary learned via GMM on PGs of the external clean image. To better illustrate the dictionary The singular values in the diagonal of \mathbf{S}_k reflect the significance of the singular vectors in \mathbf{U}_k and utilized as prior weights for weighted sparse coding which will be discussed in next section.

3.2. External Prior Guided Internal Prior Learning

After the external patch group (PG) prior is learned, we can employ it to guide the internal PG prior learning for the given testing (real noisy) image. The guidance mainly comes from two aspects. One aspect is that the external prior can guide the internal noisy PGs to be assigned to most suitable Gaussians or subspaces. And for each subspace, the other aspect is to guide the orthogonal dictionary learning of internal noisy PGs.

3.2.1 Internal Subspace Selection

Given a real noisy image, assume we can totally extract N local patches from it. Similar to the external prior learning stage, for the n -th local patch ($n = 1, \dots, N$), we extract its M most similar patches around it to form a noisy PG denoted by $\mathbf{Y}_n = \{\mathbf{y}_{n,1}, \dots, \mathbf{y}_{n,M}\}$. Then the group mean of \mathbf{Y}_n , denoted by $\boldsymbol{\mu}_n$, is calculated and subtracted from each patch by $\bar{\mathbf{y}}_{n,m} = \mathbf{y}_{n,m} - \boldsymbol{\mu}_n$, leading to the mean subtracted PG $\bar{\mathbf{Y}}_n \triangleq \{\bar{\mathbf{y}}_{n,m}\}_{m=1}^M$. For adaptivity, we project the PG $\bar{\mathbf{Y}}_n$ into its most suitable Gaussian component (subspace) of the GMM learned on external PGs. The subspace most suitable for $\bar{\mathbf{Y}}_n$ is selected by firstly calculating the posterior probability of “ $\bar{\mathbf{Y}}_n$ belonging to the k -th Gaussian component”:

$$P(k|\bar{\mathbf{Y}}_n) = \frac{\prod_{m=1}^M \mathcal{N}(\bar{\mathbf{y}}_{n,m} | \mathbf{0}, \boldsymbol{\Sigma}_k)}{\sum_{l=1}^K \prod_{m=1}^M \mathcal{N}(\bar{\mathbf{y}}_{n,m} | \mathbf{0}, \boldsymbol{\Sigma}_l)} \quad (3)$$

324 for $k = 1, \dots, K$, and then choosing the component with the
 325 maximum A-posteriori (MAP) probability $\max_k P(k|\bar{\mathbf{Y}}_n)$.
 326

327 3.2.2 Internal Orthogonal Dictionary Learning

328 Assume we have assigned all internal noisy PGs $\{\bar{\mathbf{Y}}_n\}_{n=1}^N$
 329 to their corresponding most suitable Gaussians or subspaces
 330 in $\{\mathcal{N}(\mathbf{0}, \Sigma_k)\}_{k=1}^K$. For the k -th subspace, assume the
 331 noisy PGs assigned to it are $\{\bar{\mathbf{Y}}_{k,n}\}_{n=1}^{N_k}$ such that $\bar{\mathbf{Y}}_{k,n} =$
 332 $[\bar{\mathbf{y}}_{k,n,1}, \dots, \bar{\mathbf{y}}_{k,n,M}]$ and $\sum_{k=1}^K N_k = N$. We utilize the external
 333 orthogonal dictionary \mathbf{U}_k (Eqn. (2)) to guide the learning
 334 of an orthogonal dictionary for adaptively characterizing
 335 the internal PGs in the k -th subspace. The reasons we
 336 aim to learn orthogonal dictionaries are two-fold: firstly,
 337 given an orthonormal dictionary \mathbf{D} , its quality measure *mutual incoherence*
 338 $\mu(\mathbf{D}) = \max_i \frac{|\mathbf{d}_i^\top \mathbf{d}_j|}{\|\mathbf{d}_i\|_2 \|\mathbf{d}_j\|_2}$ is naturally 0
 339 and therefore better than other redundant dictionaries; sec-
 340 ondly, the orthogonality of dictioanry can guarantee the dic-
 341 tionary learning stage has closed-form solutions (please refer
 342 to Eqn. (9)) and the closed-form solutions will make our
 343 proposed method efficient, which will be discussed in ex-
 344 perimental section.
 345

346 The learned dictionary $\mathbf{D}_k \triangleq [\mathbf{D}_{k,e} \ \mathbf{D}_{k,i}] \in \mathbb{R}^{3p^2 \times 3p^2}$
 347 has two parts: the external part $\mathbf{D}_{k,e} = \mathbf{U}_k(:, 1 : 3p^2 - r) \in$
 348 $\mathbb{R}^{3p^2 \times (3p^2 - r)}$ is directly obtained from the external dictio-
 349 nary \mathbf{U}_k , and the internal part $\mathbf{D}_{k,i}$ is consisted of dictio-
 350 nary atoms adaptively learned from the internal noisy PGs
 351 $\{\bar{\mathbf{Y}}_{k,n}\}_{n=1}^{N_k}$. For notation simplicity, we ignore the subspace
 352 index k and denote the noisy PGs assigned to each subspace
 353 as $\mathbf{Y} \triangleq \{\bar{\mathbf{Y}}_n\}_{n=1}^N = [\bar{\mathbf{y}}_{1,1}, \dots, \bar{\mathbf{y}}_{1,M}, \dots, \bar{\mathbf{y}}_{N,1}, \dots, \bar{\mathbf{y}}_{N,M}]$. The learning is performed under the weighted sparse coding
 355 framework proposed as follows:

$$\begin{aligned} & \min_{\mathbf{D}_i, \{\alpha_{n,m}\}} \sum_{n=1}^N \sum_{m=1}^M (\|\bar{\mathbf{y}}_{n,m} - \mathbf{D}\alpha_{n,m}\|_2^2 + \sum_{j=1}^{3p^2} \lambda_j |\alpha_{n,m,j}|) \\ & \text{s.t. } \mathbf{D} = [\mathbf{D}_e \ \mathbf{D}_i], \mathbf{D}_i^\top \mathbf{D}_i = \mathbf{I}_r, \mathbf{D}_e^\top \mathbf{D}_i = \mathbf{0}, \end{aligned} \quad (4)$$

362 where $\alpha_{n,m}$ is the sparse coefficient vector of the m -th
 363 patch $\bar{\mathbf{y}}_{n,m}$ in the n -th PG $\bar{\mathbf{Y}}_n$ and $\alpha_{n,m,j}$ is the j -th el-
 364 ement of $\alpha_{n,m}$. λ_j is the j -th regularization parameter de-
 365 fined as

$$\lambda_j = \lambda / (\sqrt{\mathbf{S}_j} + \varepsilon). \quad (5)$$

366 We employ square roots of the singular values in \mathbf{S} (please
 367 refer to Eqn. (2)) as external prior weights and add a small
 368 positive number ε to avoid zero denominator. Noted that
 369 $\mathbf{D}_e = \emptyset$ if $r = 3p^2$ and $\mathbf{D}_e = \mathbf{U}_k$ if $r = 0$. The dictionary
 370 $\mathbf{D} = [\mathbf{D}_e \ \mathbf{D}_i]$ is orthogonal by checking that:

$$\mathbf{D}^\top \mathbf{D} = \begin{bmatrix} \mathbf{D}_e^\top \\ \mathbf{D}_i^\top \end{bmatrix} [\mathbf{D}_e \ \mathbf{D}_i] = \begin{bmatrix} \mathbf{D}_e^\top \mathbf{D}_e & \mathbf{D}_e^\top \mathbf{D}_i \\ \mathbf{D}_i^\top \mathbf{D}_e & \mathbf{D}_i^\top \mathbf{D}_i \end{bmatrix} = \mathbf{I} \quad (6)$$

375 Similar to K-SVD [1], we employ an alternating iterative
 376 framework to solve the optimization problem (5). Specifi-
 377 cally, we initialize the orthogonal dictionary as $\mathbf{D}_{(0)} = \mathbf{U}_k$

378 and for $t = 0, 1, \dots, T - 1$, alternatively do:

379 **Updating Sparse Coefficient:** given the orthogonal dictio-
 380 nary $\mathbf{D}_{(t)}$, we update the sparse coefficient vector of the m -
 381 th patch $\bar{\mathbf{y}}_{n,m}$ in the n -th PG $\bar{\mathbf{Y}}_n$ via solving

$$\begin{aligned} \alpha_{n,m}^{(t)} &:= \arg \min_{\alpha_{n,m}} \|\bar{\mathbf{y}}_{n,m} - \mathbf{D}_{(t)} \alpha_{n,m}\|_2^2 + \sum_{j=1}^{3p^2} \lambda_j |\alpha_{n,m,j}| \\ \text{s.t. } \mathbf{D}_{(t)} &= [\mathbf{D}_e \ \mathbf{D}_i], \mathbf{D}_i^\top \mathbf{D}_i = \mathbf{I}_r, \mathbf{D}_e^\top \mathbf{D}_i = \mathbf{0}, \end{aligned} \quad (7)$$

382 Since dictionary $\mathbf{D}_{(t)} = [\mathbf{D}_e \ \mathbf{D}_i^{(t)}]$ is orthogonal, the prob-
 383 lems (7) has a closed-form solution [7]

$$\alpha_{n,m}^{(t)} = \text{sgn}(\mathbf{D}_{(t)}^\top \bar{\mathbf{y}}_{n,m}) \odot \max(|\mathbf{D}_{(t)}^\top \bar{\mathbf{y}}_{n,m}| - \Lambda, \mathbf{0}), \quad (8)$$

384 where $\Lambda = [\lambda_1, \lambda_2, \dots, \lambda_{3p^2}]$ is the vector of regulariza-
 385 tion parameter and $\text{sgn}(\bullet)$ is the sign function, \odot means
 386 element-wise multiplication.

387 **Updating Internal Dictionary:** given the sparse coeffi-
 388 cient vectors $\mathbf{A}^{(t)} = [\alpha_{1,1}^{(t)}, \dots, \alpha_{1,M}^{(t)}, \dots, \alpha_{N,1}^{(t)}, \dots, \alpha_{N,M}^{(t)}]$,
 389 we update the internal orthogonal dictionary via solving

$$\begin{aligned} \mathbf{D}_i^{(t+1)} &:= \arg \min_{\mathbf{D}_i} \sum_{n=1}^N \sum_{m=1}^M (\|\bar{\mathbf{y}}_{n,m} - \mathbf{D}_i \alpha_{n,m}^{(t)}\|_2^2) \\ &= \arg \min_{\mathbf{D}_i} \|\mathbf{Y} - \mathbf{D} \mathbf{A}^{(t)}\|_F^2 \end{aligned} \quad (9)$$

$$\text{s.t. } \mathbf{D} = [\mathbf{D}_e \ \mathbf{D}_i], \mathbf{D}_i^\top \mathbf{D}_i = \mathbf{I}_r, \mathbf{D}_e^\top \mathbf{D}_i = \mathbf{0},$$

403 The sparse coefficient matrix $\mathbf{A}^{(t)} = [(\mathbf{A}_e^{(t)})^\top \ (\mathbf{A}_i^{(t)})^\top]^\top$
 404 also has two parts: the external part $\mathbf{A}_e^{(t)} \in \mathbb{R}^{(3p^2-r) \times NM}$
 405 and the internal part $\mathbf{A}_i^{(t)} \in \mathbb{R}^{r \times NM}$ denote the coefficients
 406 over external dictionary \mathbf{D}_e and internal dictionary $\mathbf{D}_i^{(t)}$,
 407 respectively. According to the Theorem 4 in [26], the prob-
 408 lem (9) has a closed-form solution $\mathbf{D}_i^{(t+1)} = \mathbf{U}_i \mathbf{V}_i^\top$, where
 409 $\mathbf{U}_i \in \mathbb{R}^{3p^2 \times r}$ and $\mathbf{V}_i \in \mathbb{R}^{r \times r}$ are the orthogonal matrices
 410 obtained by the following SVD
 411

$$(\mathbf{I} - \mathbf{D}_e \mathbf{D}_e^\top) \mathbf{Y} (\mathbf{A}_i^{(t)})^\top = \mathbf{U}_i \mathbf{S}_i \mathbf{V}_i^\top. \quad (10)$$

412 The orthogonality of internal dictionary $\mathbf{D}_i^{(t+1)}$ can be
 413 checked by $(\mathbf{D}_i^{(t+1)})^\top (\mathbf{D}_i^{(t+1)}) = \mathbf{V}_i \mathbf{U}_i^\top \mathbf{U}_i \mathbf{V}_i^\top = \mathbf{I}_r$. In Figure 4 (c) and (d), we illustrate a denoised image by
 414 our proposed method and one internal orthogonal dictionary
 415 learned from PGs of the given noisy image.

416 3.3. The Denoising Algorithm

417 We evaluate the performance of the proposed framework
 418 on denoising real noisy images. The denoising is simulta-
 419 neously done with the guided internal dictionary learning
 420 process. We ignore the index $k \in \{1, \dots, K\}$ of subspace
 421 for notation simplicity. In the denoising stage, for each sub-
 422 space, the group mean vectors $\{\boldsymbol{\mu}_n\}_{n=1}^N$ of corresponding
 423 mean subtracted noisy PGs $\{\bar{\mathbf{Y}}_n\}_{n=1}^N$ are saved for recon-
 424 struction. Until now, we obtain the solutions of sparse coef-
 425 ficient vectors $\{\hat{\alpha}_{n,m}^{(T-1)}\}$ in Eqn. (8) for $n = 1, \dots, N; m =$
 426

Alg. 1: External Prior Guided Internal Prior Learning
for Real Noisy Image Denoising

Input: Noisy image \mathbf{y} , external PG prior GMM model
Output: The denoised image $\hat{\mathbf{x}}$.
Initialization: $\hat{\mathbf{x}}^{(0)} = \mathbf{y}$;
for $Ite = 1 : IteNum$ **do**
 1. Extracting internal PGs from $\hat{\mathbf{x}}^{(Ite-1)}$;
 for each PG \mathbf{Y}_n **do**
 2. Calculate group mean vector μ_n and form
 mean subtracted PG $\bar{\mathbf{Y}}_n$;
 3. Subspace selection via Eqn. (3);
end for
 for the PGs in each Subspace **do**
 4. External PG prior Guided Internal Orthogonal
 Dictionary Learning by solving (4);
 5. Recover each patch in all PGs via Eqn. (11);
end for
 6. Aggregate the recovered PGs of all subspaces to form
 the recovered image $\hat{\mathbf{x}}^{(Ite)}$;
end for

1, ..., M and the orthogonal dictionary $\mathbf{D}_{(T)} = [\mathbf{D}_e \mathbf{D}_i^{(T)}]$ in Eqn. (9). Then the m -th latent clean patch $\hat{\mathbf{y}}_{n,m}$ in the n -th PG \mathbf{Y}_n is recovered by

$$\hat{\mathbf{y}}_{n,m} = \mathbf{D}_{(T)} \hat{\alpha}_{n,m} + \mu_n, \quad (11)$$

where $n = 1, \dots, N; m = 1, \dots, M$. The latent clean image $\hat{\mathbf{x}}$ is reconstructed by aggregating all the estimated PGs. Similar to [7], we perform the above denoising procedures for several iterations for better denoising outputs. The proposed denoising algorithm is summarized in Alg. 1.

4. Experiments

In this section, we evaluate the performance of the proposed algorithm on real image denoising. To evaluation the effectiveness of the proposed framework of external prior guided internal prior learning, we compare it with the methods with only external prior or only internal prior (Section 4.3). We also compare the proposed algorithm with other state-of-the-art denoising methods [4, 5, 9, 8, 10, 11, 14, 19, 20, 22] (Section 4.4).

4.1. The Testing Datasets

The comparisons are performed on two standard datasets in which the images were captured under indoor or outdoor lighting conditions by different types of cameras and camera settings. The first dataset provided in [20] includes 20 real noisy images collected under uncontrolled outdoor environment. This dataset does not have “ground truth” images and hence the objective measurements can not be performed. In order to evaluate the compared methods on quantitative measures, we perform experiments on the sec-

ond dataset provided in [14]. It includes 17 real noisy images and corresponding mean images. The noisy images were collected under controlled indoor environment. Some samples can be found in [14]. For each image, the same scene was shot 500 times under the same camera and camera setting. The mean image of the 500 shots is roughly taken as the “ground truth”, with which the PSNR can be computed. Since the 17 images are too large (of size about $7000 \times 5000 \times 3$) and share repetitive contents, the authors in [14] performed comparison on 15 cropped images (of size $512 \times 512 \times 3$). To evaluate the compared methods on more samples, we cropped the 17 large images from [14] into 60 smaller images (of size $500 \times 500 \times 3$) including different contents. Some samples are shown in Figure 5. Note that the noise in our cropped 60 images used in [14] are different from the noise in the 15 images cropped by the authors of [14] since they are taken in different shots.

4.2. Implementation Details

Our proposed method contains two stages, the external prior learning stage and the external prior guided internal learning stage. In the first stage, we set $p = 6$ (so the patch size is $6 \times 6 \times 3$), $M = 10$ (the number of patches in a patch group (PG)), $W = 31$ (so the window size for PG searching is 31×31 , and $K = 32$ (the number of Gaussians in Gaussian Mixture Model (GMM)). We learn the external prior via GMM on about 3.6 million PGs extracted from the Kodak PhotoCD Dataset (<http://r0k.us/graphics/kodak/>), which includes 24 high quality color images. In the second stage, we set $r = 54$ (the number of internal atoms in the learned dictionaries), $\lambda = 0.001$ (the sparse regularization parameter), $T = 2$ (the number of iterations for solving problem (4)), and $IteNum = 4$ (the number of iterations for Alg. 1). All experiments are performed under the Matlab2014b environment on a machine with Intel(R) Core(TM) i7-5930K CPU of 3.5GHz and 32GB RAM.

4.3. Comparison among external, internal and external guided internal priors

In this section, we compare our proposed method on real image denoising with external prior based method (denoted as “External”) and internal prior based method (denoted as “Internal”). For the “External” method, we utilize the external dictionaries (i.e., $r = 0$ in Eqn. (5)) for denoising. For the given noisy image, we extract the PGs and then do internal subspace selection via Eqn. 3. The denoising is performed via the weighted sparse coding framework proposed in [7]. For the “Internal” method, the overall framework is similar to the method of [6]. We employ the GMM model (also with $K = 32$ Gaussians) to cluster the noisy PGs extracted from given noisy image into multiple subspaces, and for each subspace, we utilize the internal orthogonal

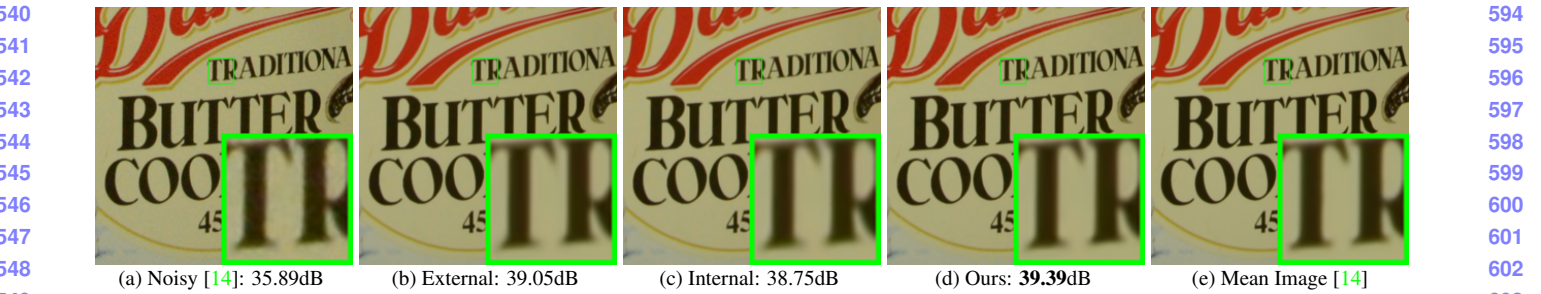


Figure 3. Denoised images of the 96-th cropped image from “Nikon D600 ISO 3200 C1” [14] by different methods. The images are better to be zoomed in on screen.

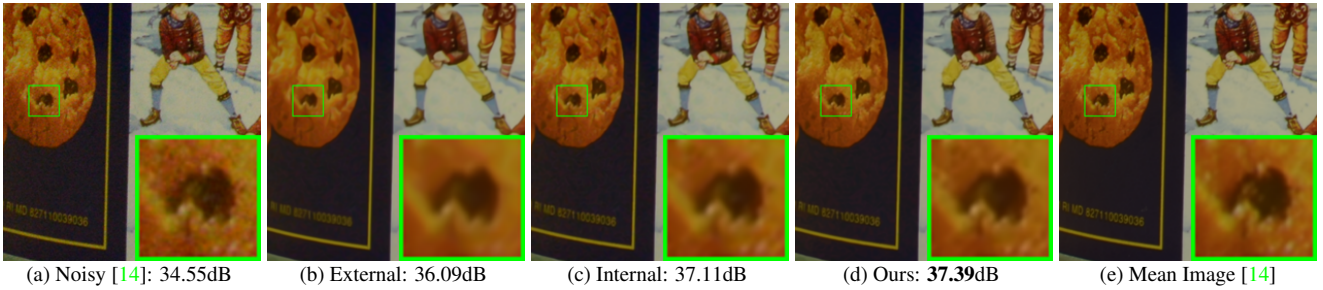


Figure 4. Denoised images of the 94-th cropped image from “Nikon D600 ISO 3200 C1” [14] by different methods. The images are better to be zoomed in on screen.



Figure 5. Some samples cropped from real noisy images of [14].

dictionary obtained via Eqn. (2) by weighted sparse coding framework in [7]. All parameters of the three methods are tuned to achieve best performance.

We compare the above mentioned methods on the 60 cropped images (of size $500 \times 500 \times 3$) from [14]. The average PSNR and speed of these methods are listed in Table 1. It can be seen that our proposed method achieves better PSNR results than the methods of “External” and “Internal”. The speed of our proposed method is much faster than the “Internal” method while only a little slower than the “External” method. We also compare the visual quality of the denoised images by these methods. From the results listed in Figure 3 and Figure 4, we can see that the “External” method is good at recovering structures (Figure 3) while the “Internal” method is good at recovering internal complex textures (Figure 4). And by utilizing both the external and internal priors, our proposed method can recover well both the structures and textures. Noted that the noisy images in Figures 3 and 4 are cropped from the same image captured by Nikon D600 at ISO = 3200 in [14]. Hence, the differences on PSNR and visual quality among these methods only depends on the contents of the cropped images.

Table 1. Average PSNR (dB) results and Run Time (seconds) of the External, the Internal, and our proposed methods on 60 real noisy images (of size $500 \times 500 \times 3$) cropped from [14].

	Noisy	External	Internal	Ours
PSNR	34.51	38.21	38.07	38.75
Time	—	39.57	667.36	43.77

4.4. Comparison with Other Denoising Methods

In this section, we compare the proposed method with other state-of-the-art image denoising methods such as BM3D [4], WNNM [8], MLP [9], CSF [10], TRD [11], Noise Clinic (NC) [19], Cross-Channel (CC) [14], and Neat Image (NI) [22]. The methods of BM3D [4], WNNM [8], MLP [9], CSF [10], and TRD [11] are designed for removing Gaussian noise. For BM3D and WNNM, the level σ of Gaussian noise is very important and is estimated by the method [27]. The other parameters are set as default. For the methods of MLP, CSF, and TRD, we employ their default parameters settings. Since these methods are designed for grayscale images, we utilize them to denoise the R, G, B channels separately for color noisy images. The Noise Clinic (NC) [19] is a blind image denoising method which does not need any noise prior. We also compare with Neat Image (NI), a commercial software for image denoising. Due to its excellent performance, Neat Image (NI) is embedded into Photoshop and Corel PaintShop [22]. The comparisons are performed on the real noisy images from [20] and [14].

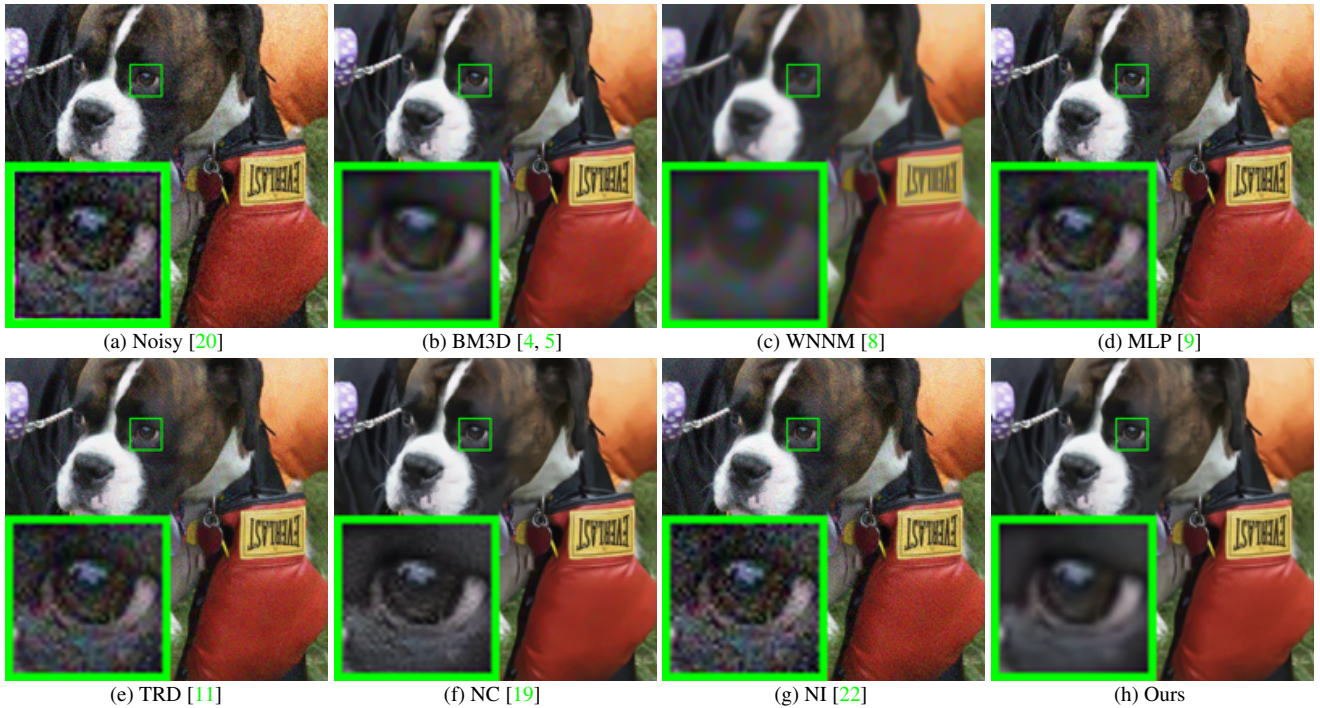


Figure 6. Denoised images of the image “Dog” by different methods. The images are better to be zoomed in on screen.

4.4.1 Comparison on the First Dataset [20]

The real noisy images in the dataset [20] do not have “ground truth” images. On this dataset, we compare the proposed method with the methods of BM3D [4], WNNM [8], MLP [9], TRD [11], Noise Clinic (NC) [19], and Neat Image (NI) [22]. We only compare the visual quality of the denoised images. Figure 6 shows the denoised images of “Dog” by the competing methods. More visual comparisons can be found in the supplementary file. It can be seen that the methods of BM3D, WNNM tend to globally over-smooth the image while locally remain some noise, while the methods of MLP, TRD are likely to remain noise in the whole image. This demonstrates that the methods designed for Gaussian noise are not effective for removing the complex noise in real noisy images. Though Noise Clinic and Neat Image are specifically developed for removing complex noise, they would sometimes fail to recover real noisy images. However, our proposed method recoveries more faithfully the structures and textures (such as the eye area) than the other competing methods.

4.4.2 Comparison on the Second Dataset [14]

The real noisy images in the second dataset [14] have corresponding “ground truth” images. On this dataset, we firstly perform comparison on the 15 cropped images used in [14]. The compared method are BM3D [4], WNNM [8], MLP [9], CSF [10], TRD [11], Noise Clinic (NC) [19], and

Cross-Channel (CC) [14]. The PSNR values are listed in Table 2. As we can see, on most (9 out of the 15) images captured by different cameras and camera settings, our proposed method obtains better PSNR values than the other methods. Noted that, though in [14] a specific model is trained for each camera and camera setting, our proposed general method still gains 0.28dB improvements on PNSR over [14]. We also compare the visual quality of the denoised images by the competing methods. Figure 7 shows the denoised images of a scene captured by Canon 5D Mark 3 at ISO = 3200 by the competing methods. More visual comparisons can be found in the supplementary file. We can see that BM3D, WNNM, NC, NI, and CC would either remain noise or generate artifacts, while MLP, TRD are likely to over-smooth the image. By combining the external and internal priors, our proposed method preserves edges and textures better than other methods.

To evaluate the compared methods on more samples, we then perform denoising experiments on the 60 smaller images cropped from the 17 images provided in [14]. The average PSNR results are listed in Table 3 (the code of [14] is not available so that it is not compared). The numbers in red color and blue color are the best and second best results, respectively. It can be seen that our proposed method achieves much better PSNR results than the other methods. The improvement of our method over the second best method (TRD) is 1dB. Due to the spacial limitations, the visual comparisions are provided in the supplementary file.

Table 2. Average PSNR(dB) results of different methods on 15 cropped real noisy images used in [14].

Camera Settings	Noisy	BM3D	WNNM	MLP	CSF	TRD	NI	NC	CC	Ours
Canon 5D Mark III ISO = 3200	37.00	37.08	37.09	33.92	35.68	36.20	37.68	38.76	38.37	40.50
	33.88	33.94	33.93	33.24	34.03	34.35	34.87	35.69	35.37	37.05
	33.83	33.88	33.90	32.37	32.63	33.10	34.77	35.54	34.91	36.11
Nikon D600 ISO = 3200	33.28	33.33	33.34	31.93	31.78	32.28	34.12	35.57	34.98	34.88
	33.77	33.85	33.79	34.15	35.16	35.34	35.36	36.70	35.95	36.31
	34.93	35.02	34.95	37.89	39.98	40.51	38.68	39.28	41.15	39.23
Nikon D800 ISO = 1600	35.47	35.54	35.57	33.77	34.84	35.09	37.34	38.01	37.99	38.40
	35.71	35.79	35.77	35.89	38.42	38.65	38.57	39.05	40.36	40.92
	34.81	34.92	34.95	34.25	35.79	35.85	37.87	38.20	38.30	38.97
Nikon D800 ISO = 3200	33.26	33.34	33.31	37.42	38.36	38.56	36.95	38.07	39.01	38.66
	32.89	32.95	32.96	34.88	35.53	35.76	35.09	35.72	36.75	37.07
	32.91	32.98	32.96	38.54	40.05	40.59	36.91	36.76	39.06	38.52
Nikon D800 ISO = 6400	29.63	29.66	29.71	33.59	34.08	34.25	31.28	33.49	34.61	33.76
	29.97	30.01	29.98	31.55	32.13	32.38	31.38	32.79	33.21	33.43
	29.87	29.90	29.95	31.42	31.52	31.76	31.40	32.86	33.22	33.58
Average	33.41	33.48	33.48	34.32	35.33	35.65	35.49	36.43	36.88	37.16

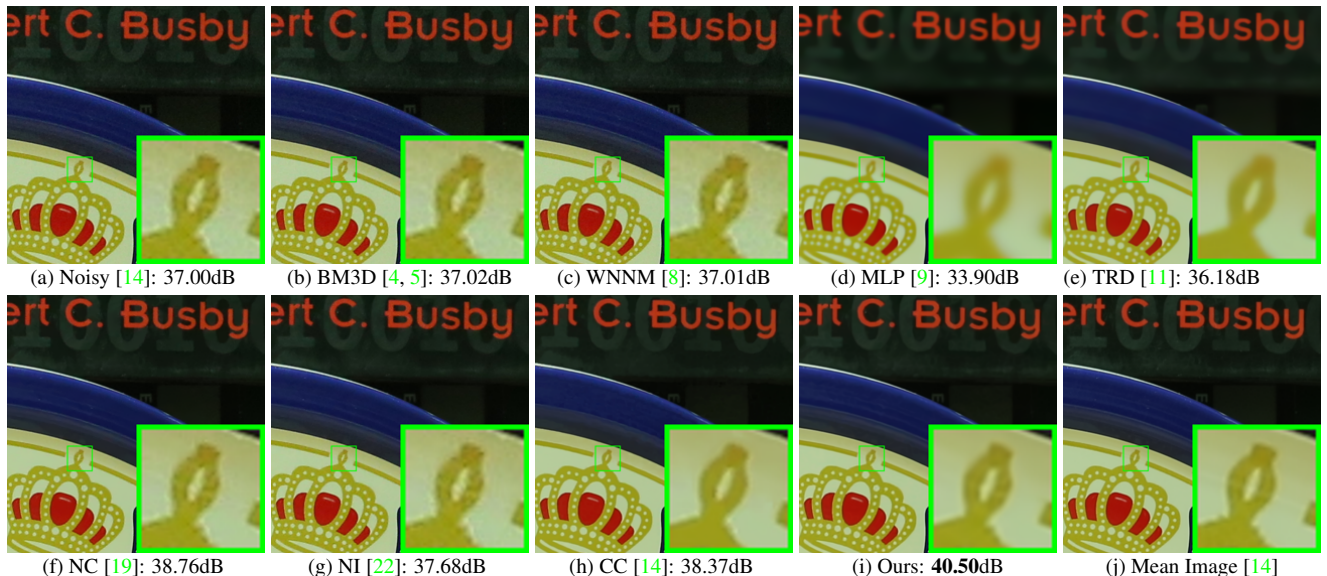


Figure 7. Denoised images of the image “Canon 5D Mark 3 ISO 3200” by different methods. The images are better to be zoomed in on screen.

Table 3. Average PSNR(dB) results of different methods on 60 real noisy images cropped from [14].

Methods	BM3D	WNNM	MLP	CSF
PSNR	34.58	34.52	36.19	37.40
Methods	TRD	NI	NC	Ours
PSNR	37.75	36.53	37.57	38.75

5. Conclusion and Future Work

Image priors are important for solving image denoising problems. The external priors learned from external clean images are generally effective to most images, while the internal priors learned directly from the noisy image are adaptive to the given image but would be biased by the com-

plex noise in real noisy images. In this paper, we demonstrates that, once unifying both the priors in external clean images and internal noisy images, we can achieve much better while still efficient performance on real image denoising problem. Specifically, the external patch group (PG) priors learned on natural clean images can be used to guide the subspace selection and orthogonal dictionary learning of internal noisy PGs from given noisy images. The experiments on real image denoising problem have demonstrated the powerful ability of the proposed method. In the future, we will speed up the proposed algorithm and evaluate the proposed method on other computer vision tasks such as image super-resolution.

864
865
866
867
868
869

References

- [1] M. Elad and M. Aharon. Image denoising via sparse and redundant representations over learned dictionaries. *IEEE Transactions on Image Processing*, 15(12):3736–3745, 2006. 1, 3, 4
- [2] J. Mairal, F. Bach, J. Ponce, G. Sapiro, and A. Zisserman. Non-local sparse models for image restoration. *IEEE International Conference on Computer Vision (ICCV)*, pages 2272–2279, 2009. 1
- [3] A. Buades, B. Coll, and J. M. Morel. A non-local algorithm for image denoising. *IEEE Conference on Computer Vision and Pattern Recognition (CVPR)*, pages 60–65, 2005. 1, 2, 3
- [4] K. Dabov, A. Foi, V. Katkovnik, and K. Egiazarian. Image denoising by sparse 3-D transform-domain collaborative filtering. *IEEE Transactions on Image Processing*, 16(8):2080–2095, 2007. 1, 2, 5, 7, 8, 9
- [5] K. Dabov, A. Foi, V. Katkovnik, and K. Egiazarian. Color image denoising via sparse 3D collaborative filtering with grouping constraint in luminance-chrominance space. *IEEE International Conference on Image Processing (ICIP)*, pages 313–316, 2007. 1, 2, 5, 7, 9
- [6] W. Dong, L. Zhang, G. Shi, and X. Li. Nonlocally centralized sparse representation for image restoration. *IEEE Transactions on Image Processing*, 22(4):1620–1630, 2013. 1, 3, 6
- [7] J. Xu, L. Zhang, W. Zuo, D. Zhang, and X. Feng. Patch group based nonlocal self-similarity prior learning for image denoising. *IEEE International Conference on Computer Vision (ICCV)*, pages 244–252, 2015. 1, 2, 3, 4, 5, 6
- [8] S. Gu, L. Zhang, W. Zuo, and X. Feng. Weighted nuclear norm minimization with application to image denoising. *IEEE Conference on Computer Vision and Pattern Recognition (CVPR)*, pages 2862–2869, 2014. 1, 2, 5, 7, 8, 9
- [9] H. C. Burger, C. J. Schuler, and S. Harmeling. Image denoising: Can plain neural networks compete with BM3D? *IEEE Conference on Computer Vision and Pattern Recognition (CVPR)*, pages 2392–2399, 2012. 1, 2, 5, 7, 8, 9
- [10] U. Schmidt and S. Roth. Shrinkage fields for effective image restoration. *IEEE Conference on Computer Vision and Pattern Recognition (CVPR)*, pages 2774–2781, June 2014. 1, 2, 5, 7, 8
- [11] Y. Chen, W. Yu, and T. Pock. On learning optimized reaction diffusion processes for effective image restoration. *IEEE Conference on Computer Vision and Pattern Recognition (CVPR)*, pages 5261–5269, 2015. 1, 2, 5, 7, 8, 9
- [12] S. Roth and M. J. Black. Fields of experts. *International Journal of Computer Vision*, 82(2):205–229, 2009. 1
- [13] D. Zoran and Y. Weiss. From learning models of natural image patches to whole image restoration. *IEEE International Conference on Computer Vision (ICCV)*, pages 479–486, 2011. 1, 3
- [14] S. Nam, Y. Hwang, Y. Matsushita, and S. J. Kim. A holistic approach to cross-channel image noise modeling and its application to image denoising. *IEEE Conference on Computer Vision and Pattern Recognition (CVPR)*, pages 1683–1691, 2016. 1, 2, 3, 5, 6, 7, 8, 9 918
919
920
921
922
923
924
925
926
927
928
929
930
931
932
933
934
935
936
937
938
939
940
941
942
943
944
945
946
947
948
949
950
951
952
953
954
955
956
957
958
959
960
961
962
963
964
965
966
967
968
969
970
971
- [15] G. E Healey and R. Kondepudy. Radiometric CCD camera calibration and noise estimation. *IEEE Transactions on Pattern Analysis and Machine Intelligence*, 16(3):267–276, 1994. 1
- [16] S. J. Kim, H. T. Lin, Z. Lu, S. Ssstrunk, S. Lin, and M. S. Brown. A new in-camera imaging model for color computer vision and its application. *IEEE Transactions on Pattern Analysis and Machine Intelligence*, 34(12):2289–2302, 2012.
- [17] C. Liu, R. Szeliski, S. Bing Kang, C. L. Zitnick, and W. T. Freeman. Automatic estimation and removal of noise from a single image. *IEEE Transactions on Pattern Analysis and Machine Intelligence*, 30(2):299–314, 2008. 1, 3
- [18] Z. Gong, Z. Shen, and K.-C. Toh. Image restoration with mixed or unknown noises. *Multiscale Modeling & Simulation*, 12(2):458–487, 2014. 1, 3
- [19] M. Lebrun, M. Colom, and J.-M. Morel. Multiscale image blind denoising. *IEEE Transactions on Image Processing*, 24(10):3149–3161, 2015. 1, 2, 3, 5, 7, 8, 9
- [20] M. Lebrun, M. Colom, and J. M. Morel. The noise clinic: a blind image denoising algorithm. <http://www.ipol.im/pub/art/2015/125/>. Accessed 01 28, 2015. 1, 3, 5, 7
- [21] F. Zhu, G. Chen, and P.-A. Heng. From noise modeling to blind image denoising. *IEEE Conference on Computer Vision and Pattern Recognition (CVPR)*, June 2016. 1, 3
- [22] Neatlab ABSsoft. Neat Image. <https://neatvideo.com/home>. 1, 2, 3, 5, 7, 9
- [23] Maria Zontak, Inbar Mosseri, and Michal Irani. Separating signal from noise using patch recurrence across scales. *Proceedings of the IEEE Conference on Computer Vision and Pattern Recognition*, pages 1195–1202, 2013. 3
- [24] G. Yu, G. Sapiro, and S. Mallat. Solving inverse problems with piecewise linear estimators: From Gaussian mixture models to structured sparsity. *IEEE Transactions on Image Processing*, 21(5):2481–2499, 2012. 3
- [25] M. Lebrun, A. Buades, and J. M. Morel. A nonlocal Bayesian image denoising algorithm. *SIAM Journal on Imaging Sciences*, 6(3):1665–1688, 2013. 3
- [26] H. Zou, T. Hastie, and R. Tibshirani. Sparse principal component analysis. *Journal of Computational and Graphical Statistics*, 15(2):265–286, 2006. 5
- [27] X. Liu, M. Tanaka, and M. Okutomi. Single-image noise level estimation for blind denoising. *IEEE transactions on Image Processing*, 22(12):5226–5237, 2013. 7